THE JOURNAL OF PHYSICAL CHEMISTRY B

Article

pubs.acs.org/JPCB

Molecular Simulation of Aqueous Electrolyte Solubility. 3. Alkali-Halide Salts and Their Mixtures in Water and in Hydrochloric Acid

Filip Moučka,[†,‡] Martin Lísal,[‡,§] and William R. Smith*[,†]

[†]Faculty of Science, University of Ontario Institute of Technology, Oshawa, ON L1H7K4, Canada

[‡]Department of Physics, Faculty of Science, J. E. Purkinje University, 400 96 Ústí n. Lab., Czech Republic

[§]E. Hála Laboratory of Thermodynamics, Institute of Chemical Process Fundamentals of the ASCR, v. v. i., 165 02 Prague 6, Czech Republic

ABSTRACT: We extend the osmotic ensemble Monte Carlo (OEMC) molecular simulation method (Moučka et al. *J. Phys Chem. B* **2011**, *115*, 7849−7861) for directly calculating the aqueous solubility of electrolytes and for calculating their chemical potentials as functions of concentration to cases involving electrolyte hydrates and mixed electrolytes, including invariant points involving simultaneous precipitation of several solutes. The method utilizes a particular semigrand canonical ensemble, which performs simulations of the solution at a fixed number of solvent molecules, pressure, temperature, and specified overall electrolyte chemical potential. It avoids calculations for the solid phase, incorporating available solid chemical potential data from thermochemical tables, which are based on well-defined reference states, or from other sources. We apply the method to a range of alkali halides in water and to selected examples involving LiCl monohydrate, mixed electrolyte solutions involving water and hydrochloric acid, and invariant points in these solvents. The method uses several existing force-field models from the literature, and the results are compared with experiment. The calculated results agree qualitatively well with the experimental trends and are of reasonable accuracy. The accuracy of the calculated solubility is highly dependent on the solid chemical potential value and also on the force-field model used. Our results indicate that pairwise additive effective force-field models developed for the solution phase are unlikely to also be good models for the corresponding crystalline solid. We find that, in our OEMC simulations, each ionic force-field model is characterized by a limiting value of the total solution chemical potential and a corresponding aqueous concentration. For higher values of the imposed chemical potential, the solid phase in the simulation grows in size without limit.

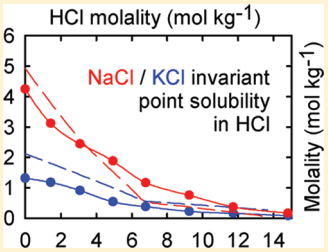

1. INTRODUCTION

This series of papers is focused on the development and application of computationally efficient algorithms for the molecular-level simulation of solutions of electrolytes and their mixtures in water and in water and another solvent. In previous papers,[1,2] we developed the basic formalism for the osmotic ensemble Monte Carlo (OEMC) simulation method, a new algorithm for directly calculating the solubility of electrolytes and their chemical potential vs concentration curves in solution, and applied it to aqueous NaCl under ambient conditions. The method employs a type of semigrand canonical ensemble, requiring only simulations of the solution phase and avoiding calculations for the solid phase, by incorporating readily available data from thermochemical tables that are based on well-defined reference states, or from other sources.

In this paper, we apply the OEMC methodology to a range of alkali halides, employing several force-field models from the literature for each, and extend it to the calculation of the solubility of electrolyte hydrates and to the mutual solubility of salts with a common ion, including their simultaneous solubility. In addition to solubility in water, we also consider solubility in hydrochloric acid, mixtures of water and HCl. Our OEMC solubility calculations incorporate thermochemical table data for the solids. We also consider results obtained by simulation of the crystalline solid using the same force field as employed in the solution phase, and preliminarily explore some details of precipitation phenomena that arise in the OEMC simulations.

2. METHODOLOGY

In this section, we briefly summarize the basis of the OEMC simulation method and extend it to the case of electrolyte hydrates and to the simultaneous solubility of two or more electrolytes in water and in a solvent involving water and another solvent such as HCl. For simplicity, we initially consider in the following only 1:1 electrolytes in aqueous solution. We summarize the OEMC method for this case and then extend it to electrolyte hydrates and to mutual and simultaneous solubility of multiple electrolytes. For more details, we refer the reader to our previous papers.[1,2]

The OEMC method simulates a solution containing t species at specified pressure P and absolute temperature T. The chemical potentials per particle $\{\mu_i\}_{i=1}^{s}$ of a subset of s species are specified by one or more relationships involving them, and the particle numbers $\{N_i\}_{i=s+1}^{t}$ of the remaining species are fixed. An example is an aqueous solution of s ions with a fixed

Received: February 13, 2012
Revised: April 4, 2012
Published: April 4, 2012

quantity of solvent species, in which the ions are in equilibrium with an external solid (additional speciation reactions of the ions are readily incorporated). The goal is to calculate the particle numbers of the s species, $S = \{N_i\}_{i=1}^{s}$.

During the simulation, a sequence of configurations is generated as in the case of a standard constant particle count, pressure, temperature (NPT) Monte Carlo (MC) simulation, with an additional MC step changing the particle numbers in S by $\Delta S = \{\Delta N_i\}_{i=1}^{s}$. This additional step is governed by the acceptance probability:

$$\Pi(i \rightarrow j) = \min\left\{1; \left[\prod_{i=1}^{s} \frac{N_i!}{(N_i + \Delta N_i)!}(V\beta P^0)^{\Delta N_i}\right] \times \exp[-\beta(\Delta U + \Delta G^p)]\right\} \quad (1)$$

where V is the volume of the system, $\beta = 1/(k_B T)$, k_B is Boltzmann's constant, P^0 is the standard-state pressure (typically 1 bar), ΔU is the configurational energy change due to the MC step, and

$$\Delta G^p = -\sum_{i=1}^{s} (\mu_i - \mu_i^0)\Delta N_i \quad (2)$$

is an externally prescribed free energy driving force, where μ_i and μ_i^0 are, respectively, the total chemical potential and the ideal-gas standard chemical potential per particle of species i. Values of the ideal-gas standard molar chemical potentials, $\tilde{\mu}_i^0 = N_A\mu_i^0$ (N_A is Avogadro's number), are typically available in thermochemical compilations such as the NIST-JANAF,[3] Thermodynamics Research Center,[4] or Wagman[5] tables.

When $\{\mu_i\}_{i=1}^{s}$ is governed by the equilibrium condition for a chemical reaction (involving the s species and other thus far unspecified species), given by

$$\sum \nu_i A_i = 0 \quad (3)$$

where $\{\nu_i\}$ are stoichiometric coefficients and $\{A_i\}$ denotes the species involved, the elements of ΔS satisfy

$$\Delta N_i = \nu_i \Delta\xi, \quad i = 1, ..., s \quad (4)$$

where $\Delta\xi$ is an extent of reaction parameter for eq 3. Equation 2 then becomes

$$\Delta G^p = -\sum_{i=1}^{s} \nu_i(\mu_i - \mu_i^0)\Delta\xi \quad (5)$$

For the case of an aqueous 1:1 electrolyte solution involving aqueous ions A^+ and B^- and its solid AB(s), eq 3 corresponds to the reaction

$$AB(s) = A^+(aq) + B^-(aq) \quad (6)$$

Equilibrium for reaction 6 is achieved when

$$\mu_{AB(s)} = \mu_{A^+(aq)} + \mu_{B^-(aq)} \quad (7)$$

corresponding to $\nu_{A^+} = \nu_{B^-} = 1$, $s = 2$ in eq 4. Substituting eq 7 in eq 5 gives

$$\Delta G^p = (\mu_{A^+}^0 + \mu_{B^-}^0 - \mu_{AB(s)})\Delta\xi \quad (8)$$

$\Delta\xi = +1$ corresponds to insertion of the ions into the solution, and $\Delta\xi = -1$ corresponds to deletion.

The solid chemical potential, $\mu_{AB(s)}$, is an input parameter for the OEMC simulation in eq 8 and ultimately in eq 1. For a solubility calculation, its experimental value can be taken from thermochemical tables[3−5] if it is available, or estimated by empirical methods (e.g., ref 6), or calculated in a separate simulation of the crystalline salt. In addition, by setting $\mu_{AB}(s)$ to a sequence of values, the OEMC method can also calculate the entire chemical potential vs concentration curve of the electrolyte in the solution.

Since the acceptance probability for direct insertion/deletion of ionic species in an aqueous solution via a single MC step is virtually zero due to its associated enormous free energy change, we overcome this problem by gradually inserting/deleting the ions via a sequence of values of a coupling parameter, λ_j, corresponding to intermediate states (or fractional particles). We break a general equilibrium process corresponding to a single MC step changing the elements of S:

$$\text{initial state} \overset{\Delta G^p}{\rightleftharpoons} \text{final state} \quad (9)$$

into subprocesses, which represent transitions between neighboring λ-states corresponding to fractional particles (frac. part.), i.e.,

$$\text{initial state } (\lambda_0 = 0) \overset{\Delta G_0^p}{\rightleftharpoons} \text{frac. part. } (\lambda_1) \overset{\Delta G_1^p}{\rightleftharpoons} \text{frac. part. } (\lambda_2)... \overset{\Delta G_{M+1}^p}{\rightleftharpoons} \text{final state } (\lambda_{M+2} = 1) \quad (10)$$

where

$$\Delta G^p = \sum_{j=0}^{M+1} \Delta G_j^p \quad (11)$$

The fractional particles are coupled to the system by means of the scaled site−site interaction potential:

$$u(r, \lambda) = \lambda u(r^*) \quad (12)$$

where

$$r^* = \{r^2 + [R_s(1 - \lambda)]^2\}^{1/2} \quad (13)$$

and $u(r)$ is a potential of any form. The parameter R_s in eq 13 is chosen in practice to achieve roughly evenly distributed acceptance ratios for all intermediate λ-states. Here, we use equidistant λ-staging, i.e., $\lambda_{j+1} = \lambda_j + \Delta\lambda$, and we set ΔG_j^p according to

$$\Delta G_j^p = w_{j+1} - w_j + (\lambda_{j+1} - \lambda_j)\Delta G^p; \quad j = 0, 1, ..., M + 1 \quad (14)$$

where w_j are biasing weights assigned to the intermediate λ-states and $w_0 = w_{M+2}$. The biasing weights w_j are adjusted during the equilibration phase of the OEMC simulation by an iterative Wang−Landau (WL)[7] procedure, which ensures that MC transitions between neighboring λ-states are reasonably likely and their relative occurrences during the simulation are roughly equal.

2.1. Solubility of an Electrolyte Hydrate. A special case of the alkali halides in practice is LiCl, which forms the monohydrate crystal $LiCl{\cdot}H_2O$ under ambient conditions. The interphase chemical reaction corresponding to eq 6 for the equilibrium of $LiCl{\cdot}H_2O(s)$ with its aqueous solution is

$$LiCl{\cdot}H_2O(s) = Li^+(aq) + Cl^-(aq) + H_2O(aq) \quad (15)$$

dx.doi.org/10.1021/jp301447z | J. Phys. Chem. B 2012, 116, 5468−5478

Table 1. Lennard-Jones Well-Depth ϵ, Size σ, and Charges q for the Water and Hydronium Model Interaction Sites, Together with the Model Geometry; k_B is the Boltzmann Constant

LJ interaction	ϵ/k_B (K)	σ (Å)	charge	q (e)	geometry	
			SPC/E Water[9]			
O	78.20	3.166	O	−0.8476	O−H	1.00 Å
			H	+0.4238	H−O−H	109.47 deg
			TIP4Pew Water[10]			
O	81.89951	3.16435	M	−1.04844	O−H	0.9572 Å
			H	+0.52422	H−O−H	104.52 deg
					O−M	0.125 Å
			TIP3P Water[11]			
O	76.54182	3.15061	O	−0.834	O−H	0.9572 Å
			H	+0.417	H−O−H	109.47 deg
			TIP4P2005 Water[13]			
O	93.19965	3.1589	M	−1.1128	O−H	0.9572 Å
			H	+0.5564	H−O−H	104.52 deg
					O−M	0.1546 Å
			Kusaka H_3O^+ [14]			
O	137.91223	2.90089	O	−0.2480	O−H	0.973 Å
			H	+0.4160	H−O−H	111.6 deg
					O−M	0.1546 Å

in which case eq 8 becomes

$$\Delta G^p = (\mu^0_{Li^+} + \mu^0_{Cl^-} + \mu^0_{H_2O} - \mu_{LiCl\cdot H_2O(s)})\Delta\xi \quad (16)$$

For an electrolyte that does not form a hydrate, a reaction step involves the simultaneous insertion or deletion of an ion pair corresponding to eq 7. For a monohydrate such as $LiCl\cdot H_2O$, a reaction step involves the simultaneous insertion or deletion of an ion pair and a water molecule, corresponding to eq 15.

2.2. Simultaneous Solubility Calculations. Equations 1−16 apply with appropriate modification for any type of solvent, which may be an undersaturated solution of other alkali halides and/or other species. When L salts are in simultaneous equilibrium with their ions in solution, L reactions corresponding to eq 6 or 15 govern the dissolution processes, and a prescribed driving free energy force is associated with each of them, with each reaction requiring a MC step changing particle counts in the simulated solution.

When two alkali halide salts dissolving in water have a common ion, at a given T and P, the phase rule dictates that the maximum value of $L = 2$ solid phases occurs at a so-called invariant point, corresponding to a unique concentration pair for the salts. Thus, e.g., in the case of the simultaneous aqueous solubility of NaCl and KCl, we must consider two MC steps that change particle counts according to the reactions:

$$NaCl(s) = Na^+(aq) + Cl^-(aq) \quad (17)$$

$$KCl(s) = K^+(aq) + Cl^-(aq) \quad (18)$$

with associated prescribed free energy driving forces:

$$\Delta G^p_{NaCl} = (\mu^0_{Na^+} + \mu^0_{Cl^-} - \mu_{NaCl(s)})\Delta\xi_{NaCl} \quad (19)$$

$$\Delta G^p_{KCl} = (\mu^0_{K^+} + \mu^0_{Cl^-} - \mu_{KCl(s)})\Delta\xi_{KCl} \quad (20)$$

These processes are coupled due to the presence of the common Cl^- ion.

For computational efficiency, as for solubility calculations for a single salt, we break the MC steps corresponding to eqs 19 and 20 into sequences of intermediate subprocesses:

$$\text{initial state } (\lambda_0, \text{NaCl}) \overset{\Delta G^p_{0,NaCl}}{\rightleftharpoons} \text{frac. part. } (\lambda_{1,NaCl}) \overset{\Delta G^p_{1,NaCl}}{\rightleftharpoons} \ldots \overset{\Delta G^p_{M+1,NaCl}}{\rightleftharpoons} \text{final state } (\lambda_{M+2}, \text{NaCl}) \quad (21)$$

$$\text{initial state } (\lambda_0, \text{KCl}) \overset{\Delta G^p_{0,KCl}}{\rightleftharpoons} \text{frac. part. } (\lambda_{1,KCl}) \overset{\Delta G^p_{1,KCl}}{\rightleftharpoons} \ldots \overset{\Delta G^p_{M+1,KCl}}{\rightleftharpoons} \text{final state } (\lambda_{M+2}, \text{KCl}) \quad (22)$$

We only allow the ions of one of the salts to be inserted/deleted at a time, i.e., the processes corresponding to eqs 21 and 22 are implemented separately. In a simulation step, each is selected with equal probability 0.5, and its direction (sign of $\Delta\xi$) is also selected with equal probability 0.5. This ensures that the microscopic reversibility condition is satisfied, and also avoids problems that could be caused by mutual interactions of the fractional particles belonging to different sequences, e.g., fractional particle pairing. Furthermore, it makes the states containing only full particles and no fractional particles (nonintermediate configurations) more frequent in the total chain of generated configurations. The last feature of this approach is important, since only the nonintermediate configurations can be used for averaging of measured thermodynamic and structural properties of the solution.

3. MOLECULAR MODELS

We considered a range of alkali halide salts involving all pairwise combinations of cations $\{Li^+, Na^+, K^+, Rb^+, Cs^+\}$ and anions $\{F^-, Cl^-, Br^-, I^-\}$ except for RbF (19 in total). We modeled the electrolytes using three different sets of force fields for the alkali and halide ions developed by Joung and Cheatham[8] in conjunction with three different water models: SPC/E,[9] TIP4Pew,[10] and TIP3P,[11] hereafter referred to as models I-S, I-T4, and I-T3, respectively. These models reasonably reproduce various experimental solution properties.[2,12] In addition, we tested the I-S ionic models for Na^+ and

dx.doi.org/10.1021/jp301447z | J. Phys. Chem. B 2012, 116, 5468−5478

Table 2. Lennard-Jones Well-Depth ϵ and Size σ for the Ion Models Used[a]

ions compatible with:	SPC/E water		TIP4Pew water		TIP3P water	
LJ interaction	ϵ/k_B (K)	σ (Å)	ϵ/k_B (K)	σ (Å)	ϵ/k_B (K)	σ (Å)
Li^+	169.4524	1.4094	52.3293	1.4397	14.0850	1.8263
Na^+	177.4574	2.1595	84.7616	2.1845	44.0014	2.4393
K^+	216.2376	2.8384	140.6332	2.8331	97.4657	3.0380
Rb^+	223.9863	3.0950	217.9707	3.0451	164.9675	3.2304
Cs^+	45.2178	3.6010	198.4871	3.3640	204.5799	3.5208
F^-	3.7241	4.0215	0.7927	4.5222	1.6928	4.1035
Cl^-	6.4337	4.8305	5.8683	4.9178	17.9102	4.4777
Br^-	13.5662	4.9017	15.2865	4.9320	29.5167	4.6469
I^-	21.5301	5.2011	20.9885	5.2599	27.0138	5.0959

[a]The values of charges q are $+e$ for the cations and $-e$ for the anions. The original values are taken from Joung et al.[8] and converted to the units employed here and appropriately rounded.

Cl^-, originally developed for TIP4Pew water, for transferability to the TIP4P2005 water model.[13]

We modeled hydrochloric acid as a mixture of water, H_3O^+, and Cl^- ions, using the Cl^- model developed by Joung and Cheatham in conjunction with SPC/E water[8] and the corresponding H_3O^+ (hydronimum) model developed by Kusaka et al.[14]

The interactions between all types of particles were modeled by a sum of Lennard-Jones (LJ) interactions:

$$U_{ij,\mathrm{LJ}} = 4\varepsilon_{ij}\left[\left(\frac{\sigma_{ij}}{r_{ij}}\right)^{12} - \left(\frac{\sigma_{ij}}{r_{ij}}\right)^{6}\right] \tag{23}$$

and Coulombic interactions:

$$U_{ij,\mathrm{Coul}} = \frac{q_i q_j}{4\pi\varepsilon_0 r_{ij}} \tag{24}$$

where ε_{ij} and σ_{ij} are, respectively, the LJ well-depth and LJ size parameters, r_{ij} is the distance between the interacting sites i and j, and q_k is the charge of the interacting site k.

All the models embody a single LJ site that either coincides with the center of the oxygen atom (O) for the water and hydronium models or is at the center of the alkali and halide particles. We summarize the model parameters in Tables 1 and 2, respectively. In all cases, the cross LJ parameters ε_{ij} and σ_{ij} are expressed using the Lorentz−Berthelot mixing rules:[15]

$$\varepsilon_{ij} = \sqrt{\varepsilon_i \varepsilon_j}$$
$$\sigma_{ij} = \frac{\sigma_i + \sigma_j}{2} \tag{25}$$

where ε_k and σ_k are the LJ well-depth and size of particle k.

4. SIMULATION DETAILS

OEMC simulations were applied to aqueous solutions under ambient conditions (T = 298.15 K, P = 1 bar) in a cubic simulation box with periodic boundary conditions. We used 270 water particles in all the studied systems except for the case of hydrochloric acid, where the total number of H_3O^+ and H_2O particles was 270. The number of alkali-halide ion pairs in the box varied, depending on the studied system and the externally imposed solid chemical potential.

We used the same value of the cutoff radius for both the LJ and Coulombic interactions, r_c = 9 Å. Initially, the particles were placed on a face-centered cubic lattice and rotations of the molecules were generated randomly. The initial configuration was then equilibrated using a standard *NPT* MC simulation.[15] The probabilities of performing particular MC steps were set at (0.005, 0.1, 0.1, 0.4, 0.395) for (volume changes, λ changes, fractional ion translations, ions/water/hydronium translations, water/hydronium rotations). In eq 13, we used R_s values found by trial and error to give roughly optimal performance; these are listed in Table 3. For the WL method, $\Delta w/k_B$ was initially set to 1.81 K and histograms were zeroed when the relative occurrence of every λ-state exceeded 0.7. Iterations were terminated when $\Delta w/k_B$ became less than 7×10^{-4} K. Values of w_j were adjusted for each OEMC run. We used M = 60 equally spaced λ values for $LiCl{\cdot}H_2O$, M = 100 for LiBr and KF, and M = 20 equally spaced λ values for the other systems, with additional values at λ_0 and λ_{M+2} corresponding to the noninteracting and fully coupled ions, respectively. We treated the long-ranged Coulombic interactions using the generalized reaction field (GRF) method[16] with tinfoil boundary conditions. Equilibration for the OEMC simulations typically consisted of up to 1×10^9 MC trial moves, and production runs took about 6×10^9 MC trial moves.

Table 3. Values Used for the Parameter R_s in eq 13

salt	R_s (Å)	salt	R_s (Å)	salt	R_s (Å)	salt	R_s (Å)
LiF	2.0	LiCl	2.5	LiBr	2.7	LiI	2.8
NaF	2.5	NaCl	2.5	NaBr	2.8	NaI	3.0
KF	2.5	KCl	2.5	KBr	2.7	KI	3.0
RbF	*a*	RbCl	2.7	RbBr	2.7	RbI	3.0
CsF	2.5	CsCl	2.7	CsBr	2.7	CsI	3.0

[a]Not considered in this work due to unavailable chemical potential data for the solid.

Table 4 summarizes the ideal-gas standard molar chemical potentials from the NIST-JANAF Thermochemical Tables[3]

Table 4. Standard Molar Ideal Gas Chemical Potentials, $\tilde{\mu}^0$, Used for the OEMC Simulations, Taken from the NIST-JANAF Thermochemical Tables[3]

species	$\tilde{\mu}^0$ (kJ mol^{-1})	species	$\tilde{\mu}^0$ (kJ mol^{-1})
Li^+	648.477	F^-	−261.997
Na^+	574.317	Cl^-	−240.167
K^+	480.947	Br^-	−238.808
Rb^+	457.771	I^-	−221.488
Cs^+	426.897	H_2O	−228.582

dx.doi.org/10.1021/jp301447z | J. Phys. Chem. B 2012, 116, 5468−5478

Table 5. Solubility of Alkali-Halide Salts in Water, m, Calculated by OEMC Using Three Sets of Joung and Cheatham's Molecular Models of Ions Compatible with Three Water Models,[8] Compared with Experimental Values[17] and Results of the Henry Convention Ideal Solution Model, at T = 298.15 K, P = 1 bar, and Externally Imposed Solid Molar Chemical Potentials, $\tilde{\mu}(s)$[a]

		m (mol kg^{-1})				
salt	$\tilde{\mu}(s)$ (kJ mol^{-1})	I-S	I-T4	I-T3	experiment	ideal soln
LiF	−588.660	0.00814(10)	0.0217(10)	0.0470(10)	0.0517	0.04
NaF	−545.081	1.03(10)	1.85(20)	1.06(10)	0.9846	0.41
KF	−538.934	18.9(10)*	18.4(10)*	precipitation	17.4973	106.11
CsF	−525.377	precipitation	precipitation	precipitation	3.8168	9544.52
LiCl·H_2O	−632.044[M]	17.0(10)*	precipitation	precipitation	19.9325	*b*
NaCl	−384.024	4.74(15)	5.41(20)	precipitation	6.1533	6.28
KCl	−408.761	3.77(15)	3.60(20)	4.80(20)	4.7669	3.18
RbCl	−407.8[NBS]	6.08(15)	5.68(15)	8.35(20)	7.7632	4.46
CsCl	−414.360	precipitation	8.66(50)	11.22(50)	11.3469	6.01
LiBr	−341.630	22.8(3)*	precipitation	precipitation	20.8301	74790.71
NaBr	−349.267	7.00(15)	8.18(15)	precipitation	9.1893	28.44
KBr	−380.431	3.74(15)	4.05(15)	4.11(10)	5.6961	3.94
RbBr	−381.79[NBS]	4.55(15)	4.62(15)	4.70(15)	7.0417	3.46
CsBr	−391.41[NBS]	precipitation	4.49(10)	4.57(10)	5.7899	2.51
LiI	−269.665	precipitation	precipitation	precipitation	12.3461	3877408.1
NaI	−284.572	11.06(20)	16.30(50)	precipitation	12.2814	340.24
KI	−323.024	5.79(20)	8.22(40)	7.44(50)	8.9239	10.84
RbI	−328.86[NBS]	4.35(15)	4.49(15)	4.24(15)	7.7813	3.85
CsI	−340.58[NBS]	precipitation	3.70(10)	3.26(10)	3.2656	1.84

[a]The values for $\tilde{\mu}(s)$ were taken from the NBS tables[5] (NBS) and from Monnin et al.[18] (M) where indicated; otherwise, they were taken from the NIST-JANAF tables.[3] * denotes results for systems with poor convergence, which are discussed in the text. [b]Not applicable.

that were used for our simulations, and the second column of Table 5 gives the values and sources of $\tilde{\mu}(s)$ used for the solids.

5. RESULTS AND DISCUSSION

5.1. Alkali-Halide Salt Solubilities in H_2O. We performed OEMC solubility simulations for 19 alkali-halides in water under ambient conditions. The results are listed in Table 5 for the three molecular model sets, together with the experimental values and with values calculated using the Henry convention ideal solution model (see below, eq 27). In the special case of LiCl, results are given for its monohydrate crystal LiCl·H_2O, which is experimentally observed under ambient conditions. It is seen that the majority of our results are in reasonable agreement with the experimental values.

The results in the table labeled "precipitation" did not converge, and are discussed later. The results noted with * in Table 5 are rather rough estimates, where we observed problems with poor convergence of the simulations involving Li^+ ions, and for the KF system. We show a typical convergence profile for such a poorly converging system involving LiBr in Figure 1. This behavior is likely due to the very strong interactions between the ions in these systems, which in turn leads to ion pairing and slow convergence of the simulated ion concentrations. We show evidence of this in Figure 2, which displays the radial distribution function $g_{Li^+,O^-}(r)$ calculated in an LiBr aqueous solution using the I-S model at m = 22.8 mol kg^{-1}. In the figure, one can see a very high first peak followed by a region of very low values, corresponding to strong ion−oxygen intermolecular pairing. The original proposers of this model encountered similar problems,[12] namely, nonergodicity caused by very long residence times of the ion−water or ion−ion pairs in the model solution. To avoid the possibility of spurious results, we performed several shorter OEMC simulations starting from different initial concentrations,

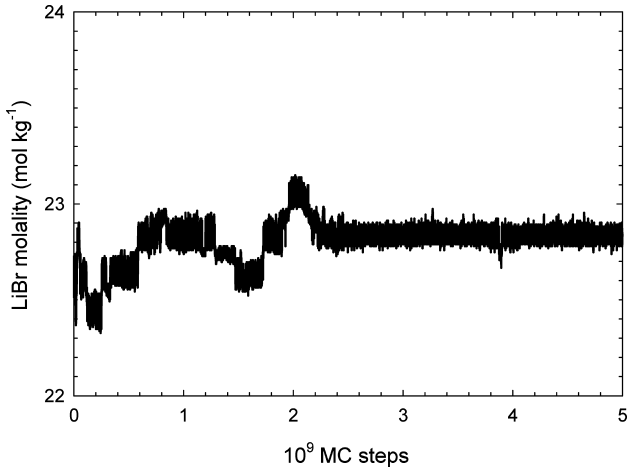

Figure 1. Convergence profile of the solubility obtained during OEMC simulation of aqueous LiBr solution at T = 298.15 K and P = 1 bar modeled by the I-S force fields.

involving values both slightly higher and slightly lower than the presented equilibrium values. All of these simulations converged, although slowly, to the value presented in Table 5.

The Henry convention ideal solution model (details of which are given in the next section) predicts reasonably well the solubilities of LiF and NaCl. The LiF solubility is fairly low, where the ideal solution model would be expected to be reasonably accurate; as noted in our previous paper,[2] the good result for NaCl is a coincidence due to the fact that the experimental activity coefficient of the ion pair is unity near the experimental solubility concentration. The Henry ideal solution model is much less accurate for the other salts, and its predicted values differ from the experimental values by an order of magnitude or more for CsF, LiBr, LiI, and NaI.

dx.doi.org/10.1021/jp301447z | J. Phys. Chem. B 2012, 116, 5468−5478

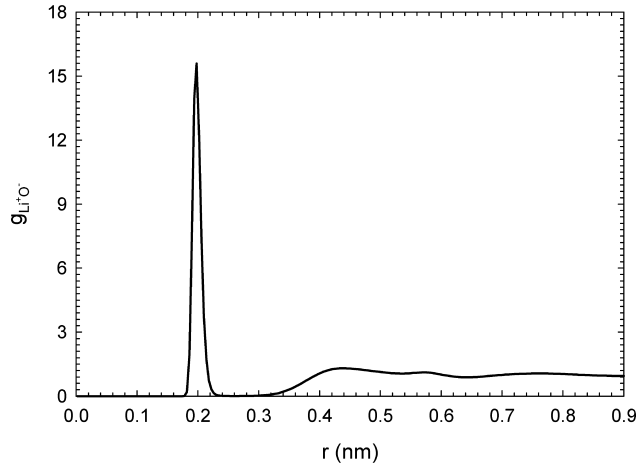

Figure 2. The radial distribution function $g_{Li^+,O^-}(r)$ calculated in an aqueous solution of LiBr simulated using the I-S model at m = 22.8 mol kg^{-1}.

The solubility values are displayed graphically and compared with experiment and with the available results of Joung and Cheatham[12] in Figure 3. The overall trends of the OEMC

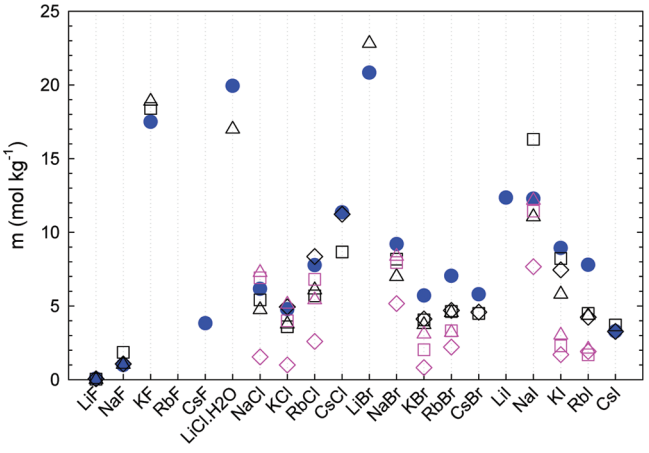

Figure 3. Graphical representation of the solubility values for the alkali halides considered in Table 5, calculated by OEMC (black symbols) for the I-S, I-T4, and I-T3 models (triangles, squares, and diamonds, respectively), and compared with the available results of Joung and Cheatham[12] (the same symbols in magenta color), and experimental values[17] (blue circles).

results are in good agreement with those of experiment, particularly considering the very strong sensitivity of solubility to the molecular model and to the specified solid chemical potential used.[2] For example, the experimental solubility trend for the salts containing Br^- follows the decreasing sequence LiBr > NaBr > RbBr > CsBr > KBr, which is generally observed in the OEMC simulations. For systems for which both OEMC and Joung and Cheatham's results are available, the best results of both approaches are in similar agreement with experiment for NaCl, KCl, RbCl, NaBr, and NaI; the OEMC results are closer to experiment for KBr, RbBr, KI, and RbI. None of the molecular models exhibit consistently better accuracy than the others.

5.2. Concentration Dependence of Chemical Potentials. In Figure 4, we display calculations of the total molar mean-ion chemical potential, $\tilde{\mu}_{NaCl}$, as a function of the electrolyte concentration, m, under ambient conditions ($\tilde{\mu} - m$ curve). The

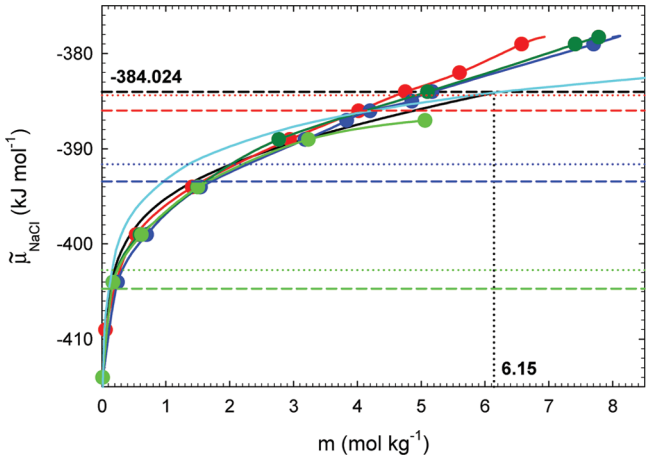

Figure 4. The molar electrolyte chemical potential $\tilde{\mu}_{NaCl}$ as a function of molality, m, for aqueous NaCl at T = 298.15 K and P = 1 bar. The red, blue, light green, cyan, and black colors represent the results obtained by OEMC using the I-S, I-T4, and I-T3 models, the Henry's convention ideal model, and the experimental values, respectively. The dark green curve denotes OEMC results obtained from Joung and Cheatham's[8] models developed for TIP4Pew water used in combination with the TIP4P2005 water model. The black dashed horizontal line denotes the solid chemical potential of NaCl, $\tilde{\mu}(s)$ = −384.024 kJ mol^{-1}.[3] The colored dashed/dotted horizontal lines represent the solid chemical potentials of NaCl calculated by thermodynamic integration for the corresponding solid (dashed and dotted for GRF and ES, respectively). The vertical dotted line denotes the experimental solubility. The curves are guides for the eye. The computed precisions of the simulation results are between 0.1 mol kg^{-1} for lower concentrations and 0.2 mol kg^{-1} for concentrations above 4 mol kg^{-1} and are not shown for the sake of clarity.

results obtained from the OEMC simulations are compared with the experimental (black) curve expressed according to the Henry convention:

$$\tilde{\mu}_{NaCl} = \tilde{\mu}^{ideal,H}_{NaCl} + 2RT \ln \gamma^{H}_{NaCl} \quad (26)$$

where R is the universal gas constant, γ^{H}_{NaCl} is the Henry convention mean-ion activity coefficient of the Na^+ and Cl^- pair in the solution given in ref 19, and $\tilde{\mu}^{ideal,H}_{NaCl}$ is the Henry convention ideal solution chemical potential:

$$\tilde{\mu}^{ideal,H}_{NaCl} = \tilde{\mu}^{\dagger}_{Na^+} + \tilde{\mu}^{\dagger}_{Cl^-} + 2RT \ln m_{NaCl} \quad (27)$$

where $\tilde{\mu}^{\dagger}_{Na^+}$ and $\tilde{\mu}^{\dagger}_{Cl^-}$ are experimentally determined values, given in the NBS thermochemical tables.[5] The results for this ideal solution chemical potential model are also shown in Figure 4 (cyan curve).

Figure 4 shows the extreme sensitivity of the solubility to the solid chemical potential, since the curves intersect its value at very small slopes. All the force-field models reproduce the experimental chemical potential curve well for $m \lesssim 3$ mol kg^{-1}. Three of them give higher results than experiment for $m \gtrsim 3$ mol kg^{-1}, whereas the (light green) I-T3 model gives results below the experimental curve in this concentration range. It is seen that the ionic models incorporated in I-T4 (blue curve) are reasonably compatible with the TIP4P2005 water model, since this combination gives the dark green $\tilde{\mu} - m$ curve very close to the IT-4 curve. The ideal solution model gives a $\tilde{\mu} - m$ curve above the experimental one at concentrations lower than 6.15 mol kg^{-1}, and it reproduces the experimental value at the solubility concentration very well; however, as noted in our previous paper,[2] this is a coincidence that does not carry over to other salts.

dx.doi.org/10.1021/jp301447z | J. Phys. Chem. B 2012, 116, 5468−5478

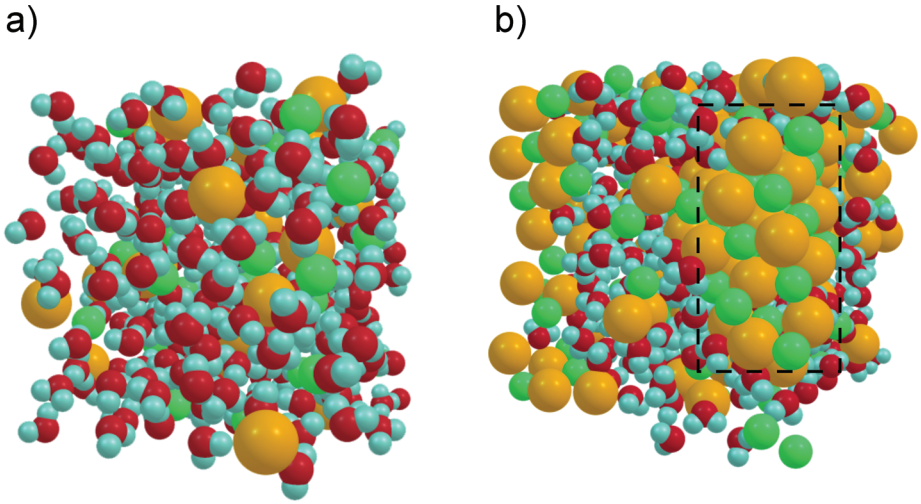

Figure 5. Snapshots of typical configurations obtained during OEMC simulations of aqueous NaCl solutions at T = 298.15 K and P = 1 bar modeled by I-T3 force fields. (a) The system at the externally imposed molar solid chemical potential $\tilde{\mu}(s)$ = −387.024 kJ mol^{-1}, with the corresponding equilibrium concentration m = 5.06 mol kg^{-1}, and (b) at $\tilde{\mu}(s)$ = −384.024 kJ mol^{-1} corresponding to a precipitating system. The red, blue, green, and yellow colors represent particles of oxygen, hydrogen, Cl^-, and Na^+, respectively. The dashed rectangle denotes the NaCl precipitate present in the simulation box.

The behavior of the $\tilde{\mu} - m$ (light green) curve for the I-T3 model is particularly interesting, and is typical of results in Table 5 indicated by "precipitation". It does not cross the experimental $\tilde{\mu}(s)$ value, appearing to terminate at a value slightly higher than $\tilde{\mu}(s) \approx -387$ kJ mol^{-1}. The simulation snapshot shown in Figure 5a demonstrates the typical liquid character of the system at $\tilde{\mu}(s)$ = −387.024 kJ mol^{-1}. For $\tilde{\mu}(s) >$ −387 kJ mol^{-1}, we observed a convergence profile typified by that of Figure 6 (calculated at $\tilde{\mu}(s)$ = −384.024 kJ mol^{-1}). Such

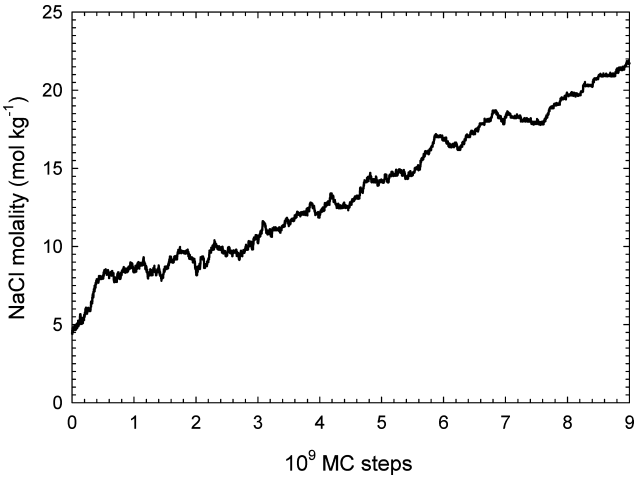

Figure 6. Convergence profile of the electrolyte molality obtained during OEMC simulation: Aqueous NaCl solution modeled by the I-T3 force-fields at ambient conditions and at the externally imposed molar solid chemical potential $\tilde{\mu}(s)$ = −384.024 kJ mol^{-1}, corresponding to a precipitating system.

simulations exhibit continuously increasing particle numbers of the ions and the formation of crystalline structures in the simulation box, as illustrated in the simulation snapshot of Figure 5b, in which the face-centered cubic crystalline structure of a NaCl precipitate is clearly recognizable. We note that the observed precipitation in our OEMC simulations is qualitatively quite different from that observed in *NPT* simulations. For the OEMC simulations, the crystal appears to grow continuously and without limit, with the system never reaching equilibrium, in contrast to the situation observed for an *NPT* simulation. The same phenomenon appears to be exhibited by all models at some limiting imposed value of the total chemical potential. This limiting value and the corresponding molality appear to be intrinsic properties of the model (and perhaps dependent on the particular system size used in the simulation). We refer to the former as the *limiting chemical potential*, $\tilde{\mu}_l$, and the latter as the *limiting concentration*, m_l, for the force-field model.

To gain further insight, we calculated the chemical potential of the corresponding solid, $\tilde{\mu}_M(s)$, for the I-T3 force-field model by thermodynamic integration (TI) using the Einstein crystal approach.[20,21] To test the correctness of our implementation of TI, we used the same computer code to perform a calculation for the Tosi−Fumi NaCl model,[22] with Ewald summation (ES) employed for handling electrostatic interactions. Our result $\tilde{\mu}_M(s)$ = −372.141 kJ mol^{-1} agrees within the simulation uncertainty with the corresponding value obtained by Sanz and Vega for the same solid model:[23] $\tilde{\mu}_M(s)$ = −372.071 kJ mol^{-1} (the value calculated by Sanz and Vega, −758.9 kJ mol^{-1}, was transformed to our scale by replacing their ideal term by the ideal term from the NIST-JANAF tables). Additionally, to verify the stability of the simulated FCC crystalline structures, we also performed *NPT* MC simulations with isotropic volume changes and Parinello−Rahman molecular dynamics simulations,[24] which allow nonisotropic volume changes; we found that the results of both approaches matched perfectly.

We present our results for $\tilde{\mu}_M(s)$ and the crystal density $\rho_M(s)$ for crystalline NaCl and KCl, obtained for the I-S, I-T4, and I-T3 models, using both the ES and the GRF methods for treating the long-ranged electrostatic forces, in Table 6, where they are compared with the experimental results.[25] (We note in passing that the $\tilde{\mu}_M(s)$ results for the ES and GRF methods do not differ significantly, suggesting that the bulk of our OEMC results, calculated in Table 5 using the GRF method for the solution phase, would only be slightly different if the ES method were used.) We also display the results for $\tilde{\mu}_M(s)$ for NaCl in the horizontal lines of Figure 4. We see that the

dx.doi.org/10.1021/jp301447z | J. Phys. Chem. B 2012, 116, 5468−5478

Table 6. NaCl and KCl Crystal Density $\rho_M(s) = m/V$ and Chemical Potential $\tilde{\mu}_M(s)$ for the Joung and Cheatham Models,[8] Calculated by Thermodynamic Integration Using Ewald Summation (ES) and the Generalized Reaction Field (GRF) Methods

	$\rho_M(s)$ (kg m^{-3})				$\tilde{\mu}_M(s)$ (kJ mol^{-1})			
method	I-S	I-T4	I-T3	expt[25]	I-S	I-T4	I-T3	expt[3]
				NaCl Crystal				
ES	2010.79(6)	2086.65(3)	2153.91(3)	2165.	−384.39	−391.62	−402.76	−384.024
GRF	2021.44(3)	2096.93(3)	2163.43(3)		−385.99	−393.42	−404.70	
				KCl Crystal				
ES	1903.17(6)	1949.75(6)	1974.23(6)	1984.	−407.30	−410.91	−417.07	−408.761
GRF	1900.31(5)	1950.34(5)	1976.11(5)		−407.70	−411.31	−417.48	

differences between the $\tilde{\mu}_M(s)$ values for the different electrolyte models are quite large, leading to large differences in the predicted solubilities using these values (as determined by the intersections of the horizontal lines of Figure 4). The order of the magnitudes of the predicted solubilities of the models is the same as the order of the magnitudes of their $\tilde{\mu}_M(s)$ values (the larger the $\tilde{\mu}_M(s)$, the larger the predicted solubility). For a given solution model, the solubility determined by $\tilde{\mu}_M(s)$ using the same force-field for the solid is referred to as the *intrinsic solubility* of the force-field. This is seen from Figure 4 to be significantly lower than the solubility values obtained by OEMC using NIST-JANAF $\tilde{\mu}_M(s)$ values for the I-T3 and I-T4 models, and only slightly lower for the I-S model (due to the fact that the $\tilde{\mu}_M(s)$ of the I-S model is (perhaps coincidentally) very close to the experimental value). The $\rho_M(s)$ values also differ considerably for the different models, and except for the I-T3 NaCl and KCl models, they differ from the experimental crystal density.

The large spread of the calculated $\tilde{\mu}_M(s)$ and $\rho_M(s)$ values in Table 6 indicates that the models are not suitable for accurate simulations of the corresponding solid salts. This is in contrast to their behavior in the aqueous phase, where the $\tilde{\mu} - m$ curves of the models do not differ mutually by more than 5 kJ mol^{-1}, even at very high concentrations. We also see from Figure 4 that the OEMC value of $\tilde{\mu}_l$ in all cases is significantly higher than the value of $\tilde{\mu}_M(s)$ calculated by TI for the crystal simulation using the same model. We suggest that the difference between $\tilde{\mu}_l$ and $\tilde{\mu}_M(s)$ for a model is related to the barrier of the nucleation free energy (see, e.g., refs 26 and 27), which can strongly depend on the simulation system size. The OEMC method avoids the problem of the inappropriateness of using the same effective molecular model for both solution and pure solid phases by employing experimentally based $\tilde{\mu}(s)$ values from thermochemical tables or from a separate crystal simulation using a more appropriate model for that phase. It also avoids the potential problem of a nucleation free energy barrier by not simultaneously simulating the liquid and solid phases (the approach used by Joung and Cheatham[12]).

Figure 7 shows $\tilde{\mu} - m$ curves and $\tilde{\mu}(s)$ values for KCl corresponding to those of Figure 4 for NaCl. All three molecular models give results very close to the experimental curve for $m \lesssim 3$ mol kg^{-1}. At higher concentrations, the calculated chemical potentials lie slightly above the experimental curve. As a result, the simulations underestimate the experimental solubilities by ≈1 mol kg^{-1} for the I-S (red curve) and I-T4 (blue curve) models, and the agreement with experiment of the result for the I-T3 (green curve) model is well within the simulation uncertainty of ≈0.2 mol kg^{-1}. We also observe that the GRF and ES results for the solid are much closer together than for NaCl. Also, in contrast to the case for

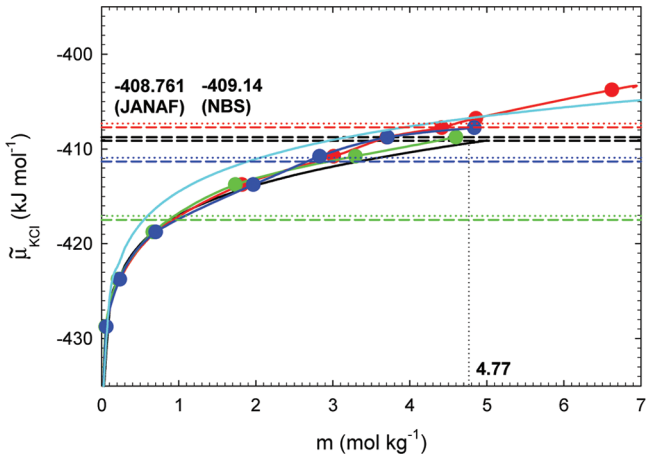

Figure 7. The molar electrolyte chemical potential $\tilde{\mu}_{KCl}$ as a function of molality m, for aqueous KCl at T = 298.15 K and P = 1 bar. The notation is the same as for Figure 4. The two black dashed lines represent values for molar solid KCl chemical potential $\tilde{\mu}(s)^{JANAF}$ = −408.761 kJ mol^{-1}[3] and $\tilde{\mu}(s)^{NBS}$ = −409.14 kJ mol^{-1}.[5] The computed precisions of the simulation results are between 0.1 and 0.2 mol kg^{-1} similarly as for Figure 4.

NaCl, $\tilde{\mu}(s)$ for the I-S model, the intrinsic solubility of 4.5 m is close to the experimental value of 4.77. The Henry convention ideal solution model (cyan curve) gives a $\tilde{\mu} - m$ curve higher than the experimental one at all concentrations, and hence predicts a lower solubility.

The solubility values predicted by Joung and Cheatham[12] for NaCl and KCl using their direct simulation approach in a slab geometry are higher than our intrinsic solubility values for all force-field models considered. However, detailed comparison of the results obtained using alternative simulation approaches for solid solubility calculations requires a separate study that is beyond the scope of this work.

5.3. NaCl and KCl Solubility in Hydrochloric Acid. In Figure 8, we illustrate OEMC calculations of electrolyte solubility in hydrochloric acid for NaCl and KCl under ambient conditions. We used the NaCl(s) and KCl(s) $\tilde{\mu}(s)$ values from Table 5 and considered a range of acid concentrations from m = 0 to 15 mol kg^{-1}. Our results (red curves) are compared with the experimental values[28] (black curves) in Figure 8a and b for NaCl and KCl, respectively. Here, we used only the I-S model, since the choice of the water force field is dictated by the compatibility requirement with Kusaka's hydronium model. The qualitative behavior of our results is very good for both systems; the calculated solubilities decrease with increasing HCl concentration, in concordance with the experimental results. The NaCl results quantitatively underestimate the experimental values for acid concentrations

dx.doi.org/10.1021/jp301447z | J. Phys. Chem. B 2012, 116, 5468−5478

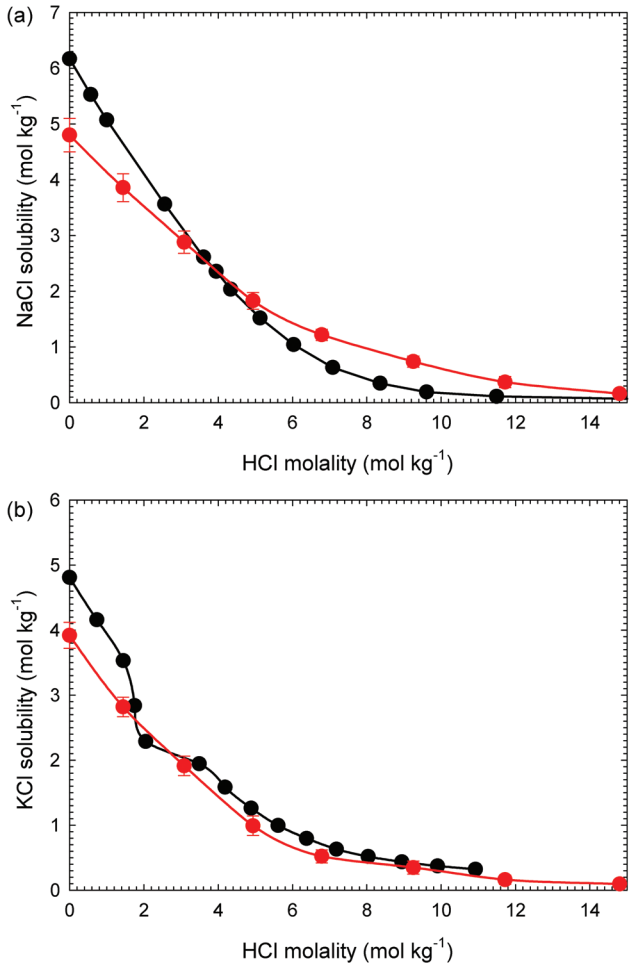

Figure 8. The solubility of NaCl (a) and of KCl (b) in hydrochloric acid as a function of acid concentration at T = 298.15 K and P = 1 bar. The red symbols represent results obtained by OEMC using the I-S models for Na^+, K^+, Cl^-, and H_2O and the Kusaka model for H_3O^+ at the externally imposed molar solid chemical potential $\tilde{\mu}(s)$ = −384.024 kJ mol^{-1} for NaCl and $\tilde{\mu}(s)$ = −408.761 kJ mol^{-1} for KCl. The black symbols represent experimental values, and the curves are guides for the eye.

$m_{HCl} \lesssim 4$ mol kg^{-1}, and are slightly higher at higher concentrations. The results for KCl lie below the experimental curve at all HCl concentrations (except near 2 mol kg^{-1}). The agreement of our results with experiment is surprisingly good, in view of the fact that the hydronium force field was not optimized to be compatibile with the force fields of the alkali and halide ions. This demonstrates good transferability of Joung and Cheatham's[8] alkali and halide models to more complex solutions. We note in passing that the experimental KCl curve exhibits anomalous behavior at $m_{HCl} \approx 2$ mol kg^{-1}, which could indicate experimental inaccuracy.

5.4. NaCl−LiCl−H_2O System. In Figure 9, the solubility of NaCl in an aqueous solution of LiCl, as calculated by our OEMC approach under ambient thermodynamic conditions, using $\tilde{\mu}_{NaCl}(s)$ = −384.024 kJ mol^{-1} and LiCl concentrations ranging from m = 0 to 15 mol kg^{-1} (red curves), is compared to experimental values[28] (black curve). The I-S (filled circles) and I-T4 (open circles) models were employed; the I-T3 model was not used, since it exhibits NaCl precipitation at the experimental solid chemical potential in pure water (see Table 5). The calculated solubilities decrease with increasing

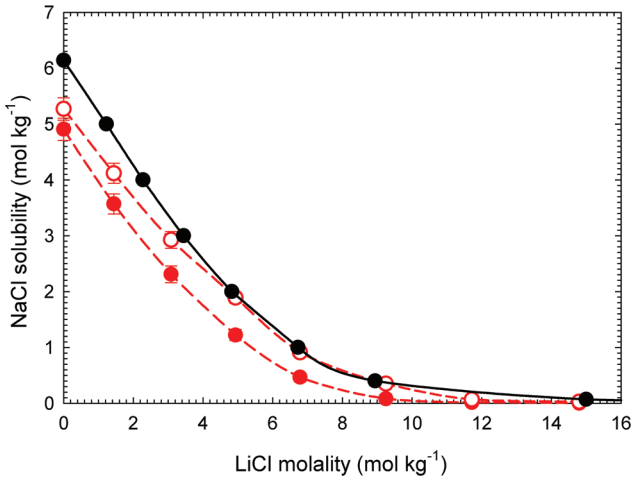

Figure 9. The solubility of NaCl in an aqueous solution of LiCl as a function of LiCl concentration at T = 298.15 K and P = 1 bar. The red symbols represent results obtained by OEMC using the I-S (filled symbols) or I-T4 model (open symbols) at the externally imposed molar solid chemical potential $\tilde{\mu}(s)$ = −384.024 kJ mol^{-1}. The black symbols represent experimental values, and the curves are guides for the eye.

LiCl concentration, in qualitative agreement with experiment. Our results lie ≈1 mol kg^{-1} below the experimental values at low LiCl concentrations, and the quantitative agreement improves with increasing LiCl concentration.

5.5. NaCl−KCl−H_2O System. As a test of the mutual compatibility of Joung and Cheatham's[8] force-fields for Na^+ and K^+ with Cl^- as the common ion, we performed OEMC simulations of NaCl and KCl simultaneously present in an aqueous solution under ambient conditions. We used the I-S and I-T4 models; the I-T3 model was again not used, since it exhibits NaCl precipitation at the experimental solid chemical potential (see Table 5). The $\tilde{\mu}(s)$ values are those given in Table 5. Figure 10 compares the OEMC solubility (dashed) curves with the experimental data[28] (black circles). Each of the two invariant points (green circles) was calculated directly by a single OEMC simulation. The branches connecting the invariant point with the vertical axis (blue curves) refer to fixed KCl concentrations, while the other branches connecting the invariant point with the horizontal axis (red curves) refer to fixed NaCl concentrations. Our OEMC results agree qualitatively with those of the experiments, with both simulation branches being roughly parallel to the corresponding experimental curve. The invariant points for both force-field models correspond to molalities ≈1 mol kg^{-1} for NaCl and ≈0.5 mol kg^{-1} for KCl lower than the experimental values.

5.6. NaCl−KCl−HCl−H_2O System. Figure 11 shows the OEMC invariant point concentrations of NaCl and KCl as functions of HCl molality (red curves), in comparison with the experimental data[28] (black curves), using the $\tilde{\mu}(s)$ values given in Table 5. Only the I-S model was employed, due to the compatibility requirement with Kusaka's hydronium model. Although this solution is relatively complex, containing five components including four ions, the OEMC simulation results predict both qualitatively well and quantitatively reasonably well the experimental behavior. The invariant point solubilities decrease with increasing HCl concentration, and the predicted NaCl invariant point concentrations are higher than those of KCl over the entire range of HCl concentrations. Both simulation results lie below the experimental curves at low

dx.doi.org/10.1021/jp301447z | J. Phys. Chem. B 2012, 116, 5468−5478

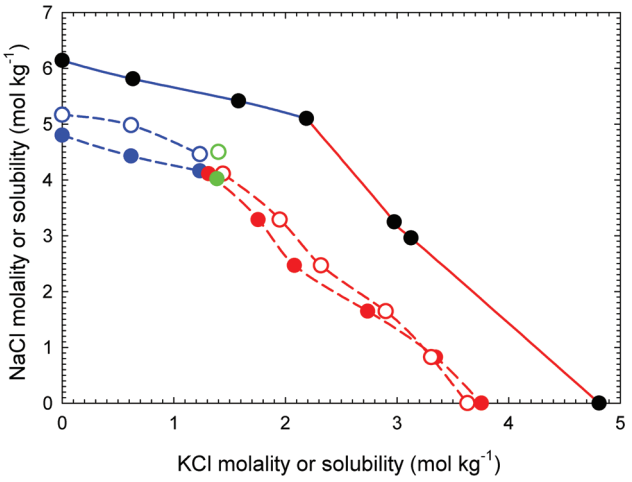

Figure 10. The simultaneous/mutual solubility curve for NaCl and KCl in water at T = 298.15 K and P = 1 bar. Colored symbols represent results obtained by OEMC, and black symbols represent experimental values. The blue, red, and green colors respectively denote NaCl solubility at a given KCl concentration, KCl solubility at a given NaCl concentration, and the invariant point. For H_3O^+, Kusaka's model was used; for Na^+, Cl^-, and H_2O, the I-S model (filled symbols) or the I-T4 model (open symbols) was employed. The curves are guides for the eye. The statistical uncertainties of the simulation results are about 0.2 mol kg^{-1}. The experimental invariant point lies at $(\tilde{\mu}_{NaCl}, \tilde{\mu}_{KCl})$ = (5.10, 2.19). The corresponding results for the I-S and I-T4 models are, respectively, (4.0, 1.4) and (4.5, 1.4).

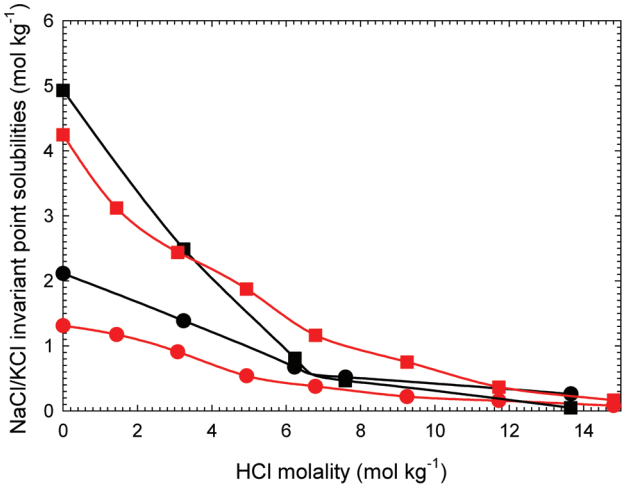

Figure 11. The simultaneous solubility of NaCl (squares) and KCl (circles) in hydrochloric acid as a function of the acid concentration at T = 298.15 K and P = 1 bar. The red symbols denote results obtained by OEMC using Kusaka's model for H_3O^+ and the I-S model for Na^+, Cl^-, and H_2O. The black color denotes experimental values. The curves are guides for the eye. The statistical uncertainties of the simulation results are about 0.2 mol kg^{-1}.

concentrations; the simulation curve for NaCl crosses above the experimental one at $m \approx 2.8$ mol kg^{-1}.

6. CONCLUSIONS

We have extended the OEMC simulation method of part 2 of this series[2] to the cases of electrolyte hydrates and to mutual and simultaneous electrolyte solubility in more complex solutions in which the electrolytes contain a common ion. We applied the methodology to aqueous solutions of alkali-halide salts and their mixtures in aqueous and in hydrochloric acid solutions. The results demonstrate the broad applicability of the OEMC method to a range of aqueous electrolytes and the feasibility of extending it to more complex solutions, both for the direct calculation of solubility and for the calculation of the ionic chemical potential vs concentration curves.

The OEMC simulation results predict the ion chemical potentials in solution and solubility trends accurately in comparison with experiment. For NaCl−KCl aqueous mixtures, the calculated solubilities and invariant point predictions also agree reasonably well with the experimental trends. The same holds true for the concentration dependence of the corresponding invariant point in hydrochloric acid solvent, for the NaCl and KCl solubility in hydrochloric acid, and the NaCl solubility in LiCl solutions.

We observed incipient solid precipitation to be exhibited by all ion and water models for simulations at and above a particular value of the externally imposed solid chemical potential, leading to the notion of each model being characterized by a *limiting chemical potential*, $\tilde{\mu}_l$, and a corresponding *limiting concentration*, $\tilde{\mu}_l$ (both of which may be dependent on the simulation system size). At imposed chemical potential values $\tilde{\mu} > \tilde{\mu}_l$, precipitation occurs, characterized by growth of the solid phase without limit, and occurring in a qualitatively different way than in the case of *NPT* simulations. We found $\tilde{\mu}_l$ to be generally higher than the corresponding solid chemical potential, $\tilde{\mu}_M(s)$, calculated by means of a separate simulation of the pure crystal using the same ionic force-field model as for the solution. In some cases, we also found $\tilde{\mu}_l$ to be higher than the experimental value of the solid chemical potential, $\tilde{\mu}(s)$, although this is dependent on the model. The fact that $\tilde{\mu}_l > \tilde{\mu}_M(s)$ is not surprising, since the aqueous system must overcome a free energy of nucleation barrier in order to start precipitating. Solid nucleation from a liquid solution is a complex phenomenon,[26,27] suggesting that methods involving simultaneous simulation of both liquid and solid phases may be problematic; the OEMC method avoids problems connected with a nucleation barrier by avoiding the explicit simulation of the solid during a simulation.

We found the values of $\tilde{\mu}_l$ and $\tilde{\mu}_M(s)$ to depend strongly on the model, whereas the chemical potential vs concentration curves showed a much weaker dependence. Our simulations thereby provide strong evidence that a pairwise additive ionic force field model that performs well for an aqueous solution does not necessarily provide a suitable model for the corresponding crystal.

The deviations of our predicted OEMC results from experimental values are not surprising, since the solubility is very sensitive to the underlying molecular model for the solution phase and to the solid chemical potential used. This is particularly true for the latter, and to a somewhat lesser extent for the former. By utilizing accurate experimental values for the solid phase chemical potential (where available), the OEMC method avoids potential problems associated with both a nucleation barrier for solid formation and with the use of an incorrect solid model. (If experimental solid phase chemical potentials are not available, then accurate values for it depend on the use of appropriate models for that phase.) Assuming accurate solid phase chemical potential values are used, improvements to the predictions will only be possible when improved force-field models become available, for both solution and solid phases.

dx.doi.org/10.1021/jp301447z | J. Phys. Chem. B 2012, 116, 5468−5478

AUTHOR INFORMATION

Notes

The authors declare no competing financial interest.

ACKNOWLEDGMENTS

Support for this work was provided by the Natural Sciences and Engineering Research Council of Canada (Grant No. OGP1041), the Ontario Research Fund, the SHARCNET grid computing facility (http://www.SHARCNET.ca), the Grant Agency of the Czech Republic (Grant No. 203/08/0094), the Grant Programme of the Ministry of Education, Youth and Sports of the Czech Republic (Project KONTAKT II LH1020), and the European Community under the seventh Framework Programme (Project COST TD0802).

REFERENCES

(1) Lísal, M.; Smith, W. R.; Kolafa, J. *J. Phys. Chem. B* **2005**, *109*, 12956−12965.
(2) Moučka, F.; Lísal, M.; Škvor, J.; Jirsák, J.; Nezbeda, I.; Smith, W. R. *J. Phys. Chem. B* **2011**, *115*, 7849−7861.
(3) Chase, M., Jr. *NIST-JANAF Thermochemical Tables*; J. Phys. and Chem. Reference Data Monograph No. 9, Am. Chem. Society, Am. Inst. Physics: 1998.
(4) Pedley, J. B. *Thermodynamical Data and Structures of Organic Compounds*; TRC Data Series; Thermodynamic Research Center: College Station, TX: 1994.
(5) Wagman, D. D.; et al. *J. Phys. Chem. Ref. Data* **1982**, *11*, Suppl. 2.
(6) Joback, K. G.; Reid, R. C. *Chem. Eng. Commun.* **1987**, *57*, 233−243.
(7) Wang, F.; Landau, D. P. *Phys. Rev. Lett.* **2001**, *86*, 2050−2053.
(8) Joung, I. S.; Cheatham, T. E., III. *J. Phys. Chem. B* **2008**, *112*, 9020−9041.
(9) Berendsen, H. J. C.; Grigera, J. R.; Straatsma, T. P. *J. Phys. Chem.* **1987**, *91*, 6269−6271.
(10) Horn, W. H.; Swope, W. C.; Pitera, J. D.; Madura, J. D.; Dick, T. J.; Hura, G. L.; Head-Gordon, T. *J. Chem. Phys.* **2004**, *120*, 9665−9678.
(11) Jorgensen, W. L.; Chandrasekhar, J.; Madura, J. D.; Impey, R. W.; Klein, M. L. *J. Chem. Phys.* **1983**, *79*, 926−935.
(12) Joung, I. S.; Cheatham, T. E., III. *J. Phys. Chem. B* **2009**, *113*, 13279−13290.
(13) Abascal, J. L. F.; Vega, C. *J. Chem. Phys.* **2005**, *123*, 234505−234517.
(14) Kusaka, I.; Wang, Z.-G.; Seinfeld, J. H. *J. Chem. Phys.* **1998**, *108*, 6829−6848.
(15) Allen, M. P.; Tildesley, D. J. *Computer Simulation of Liquids*; Clarendon Press: Oxford, U.K., 1987.
(16) Hummer, G.; Pratt, L. R.; García, A. E. *J. Phys. Chem.* **1996**, *100*, 1206−1215.
(17) Haynes, W. M. *CRC Handbook of Chemistry and Physics*, 91st ed., Internet Version 2011, http://www.hbcpnetbase.com/.
(18) Monnin, Ch.; Dubois, M.; Papaiconomou, N.; Simonin, J.-P. *J. Chem. Eng. Data* **2002**, *47*, 1331−1336.
(19) Hamer, W. J.; Wu, Y.-C. *J. Phys. Chem. Ref. Data* **1972**, *1*, 1047−1099.
(20) Frenkel, D.; Ladd, A. J. C. *J. Chem. Phys.* **1984**, *81*, 3188−3193.
(21) Anwar, J.; Frenkel, D.; Noro, M. G. *J. Chem. Phys.* **2003**, *118*, 728−735.
(22) Fumi, F.; Tosi, M. *J. Phys. Chem. Solids* **1964**, *25*, 31−43.
(23) Sanz, E.; Vega, C. *J. Chem. Phys.* **2007**, *126*, 014507.
(24) Parrinello, M.; Rahman, A. *Phys. Rev. lett.* **1980**, *45*, 1196−1199.
(25) http://www.saltinstitute.org/About-salt/Physical-properties.
(26) Desgranges, C.; Delhommelle, J. *J. Am. Chem. Soc.* **2006**, *128*, 10368−10369.
(27) Koishi, T.; Kenji, Y.; Ebisuzaki, T. *J. Chem. Phys.* **2003**, *119*, 11298−11305.
(28) Linke, W. F.; Seidell, A. *Solubilities of Inorganic and Metal−Organic Compounds*; American Chemical Society: Washington, DC, 1965.